Synthesis, thermal stability, and magnetic properties of a manganese(II) coordination framework containing bistriazolate ligands

Hana Bunzen, Maciej Grzywa, Reem Aljohani, Hans-Albrecht Krug von Nidda, Dirk Volkmer

Angaben zur Veröffentlichung / Publication details:

Bunzen, Hana, Maciej Grzywa, Reem Aljohani, Hans-Albrecht Krug von Nidda, and Dirk Volkmer. 2019. "Synthesis, thermal stability, and magnetic properties of a manganese(II) coordination framework containing bistriazolate ligands." *European Journal of Inorganic Chemistry* 2019 (41): 4471–76. https://doi.org/10.1002/ejic.201900796.

ChemPubSoc Europe

DOI: 10.1002/ejic.201900796

EurJIC European Journal of Inorganic Chemistry

Full Paper

Magnetic Coordination Polymers

Synthesis, Thermal Stability, and Magnetic Properties of a Manganese(II) Coordination Framework Containing Bistriazolate Ligands

Hana Bunzen,*[a] Maciej Grzywa,[a] Reem Aljohani,[a] Hans-Albrecht Krug von Nidda,[b] and Dirk Volkmer*[a]

Abstract: By combining a bistriazole ligand, [1,2,3]triazolo-[4,5-*f*]benzotriazole-4,8(2*H*,6*H*)-dione ($H_2C_6N_6O_2$), and Mn(II) cations in water, we prepared a Mn(II) coordination framework having an unexpected structure. As revealed by single-crystal X-ray analysis, the compound crystallizes in the monoclinic crystal system in the space group $P2_1/n$ and forms a 2D layered structure. The complex formula is $[Mn_3(C_6N_6O_2)_2(OH)_2(H_2O)_4]$, and the framework is formed by bistriazolate and hydroxido ligands, Mn(II) cations (with two different coordination environments), and coordinated water molecules. The thermal stability was studied by TGA and VT XRPD. The studies reveal that the material is stable up to 250 °C. Furthermore, magnetic measurements show that the Mn(II) coordination framework undergoes ferrimagnetic order below 6.5 K.

Introduction

1,2,3-Triazoles and bistriazoles (Figure 1) have been shown to be very useful ligands for preparing coordination polymers[1,2] including metal-organic frameworks (MOFs).[3–9] For instance, in 2009 we reported on benzobistriazole (**1**) to form a MOF called MFU-4 containing zinc(II) cations.[10] Recently, we modified the benzobistriazole ligand by oxidizing the benzene unit to a *p*-quinone moiety in order to introduce redox-active properties (ligand **2**).[11] In another work Liao et al. reported on a MOF prepared by combining the benzobistriazole ligand (**1**) with Mn(II).[12] They showed that in the porous metal azolate framework (MAF-X25) having a honeycomb-like structure, the Mn(II) ions could be post-synthetically oxidized to Mn(III) to achieve drastic increase of catalytic oxidation performance. Later Dincă et al. reported on a structurally related MOF, based on an extended bisbenzotriazole ligand, bis(1*H*-1,2,3-triazolo[4,5-*b*],[4′,5′-*i*])dibenzo[1,4]dioxin (**3**), and Mn(II) cations.[13] This MOF, also displaying a honeycomb-like network, was shown to be useful in reversible capture of ammonia. Another triazolate ligand, benzotriazole-5-carboxylic acid (**4**), was reported to be very useful in preparing Mn(II) MOFs, especially those with interesting magnetic properties.[14,15]

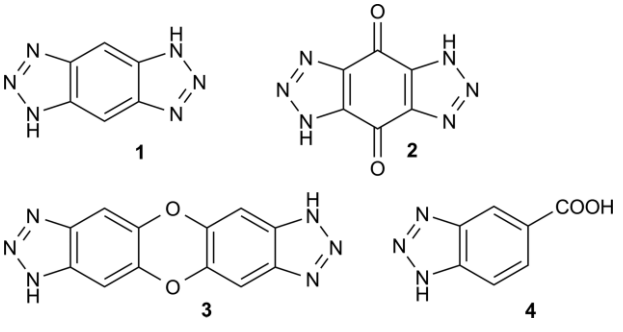

Figure 1. Examples of 1,2,3-triazole ligands used in the synthesis of coordination polymers.

In recent years coordination polymers have been used as excellent candidates to study bulk magnetic phenomena.[16–20] With regard to that, a magnetic exchange between paramagnetic metal centers is important and is primary dependent on the nature of the bridging ligand. Thus, developing coordination materials with new bridging ligands is a smart way to possibly produce materials with new, attractive magnetic properties. Inspired by these results, we intended to prepare coordination frameworks by combining the ligand **2** {[1,2,3]triazolo[4,5-*f*]benzotriazole-4,8(2*H*,6*H*)-dione} with Mn(II) cations. To our surprise, we did not obtained a MOF with a honeycomb-like structure which would be structurally related to the previously reported Mn(II) frameworks[12,13] based on the

[a] *Chair of Solid State and Materials Chemistry, Institute of Physics, University of Augsburg, Universitätsstraße 1, 86159 Augsburg, Germany*
E-mail: hana.bunzen@physik.uni-augsburg.de
dirk.volkmer@physik.uni-augsburg.de
[b] *Experimental Physics V, Center for Electronic Correlations and Magnetism, Institute of Physics, University of Augsburg, Universitätsstraße 1, 86159 Augsburg, Germany*
Supporting information and ORCID(s) from the author(s) for this article are available on the WWW under https://doi.org/10.1002/ejic.201900796.

bisbenzotriazole ligands (**1** and **3**), but instead, we obtained a two dimensional Mn(II) coordination framework. In the framework only four of the six N-donor atoms of the ligand are involved in the coordinate bonding to the Mn(II) ions. This coordination motif is, however, also different than the one often found in structurally similar imidazolate-base MOFs known as zeolitic imidazolate frameworks (ZIFs).[21,22] In the framework reported here N-donor atoms situated next to each other, namely N1 and N2, and N4 and N5, participate in the coordinate bond formation, whilst in ZIFs the N-atoms are in the positions 1 and 3 of the imidazole ring.

Results and Discussion

Synthesis of the Mn(II) Coordination Framework

The Mn(II) coordination framework was synthetized by combining the disodium salt of [1,2,3]triazolo[4,5-*f*]benzotriazole-4,8(2*H*,6*H*)-dione (**2**) and $MnCl_2{\cdot}4H_2O$ in water at 100 °C for 16 h. Upon cooling down, the compound was isolated as light yellow-orange block crystals (Figure S1, Supporting information). The same results were obtained, when we used $MnBr_2{\cdot}4H_2O$ or $Mn(OAc)_2{\cdot}4H_2O$ as metal salts suggesting that the character of the anion was not significant for the framework formation. This was later confirmed by singly crystal X-ray diffraction analysis which revealed that the framework comprised only the metal cations, organic ligand anions, and hydroxido and aqua ligands. The FTIR spectrum of the Mn(II) coordination framework was measured and compared to the spectrum of the ligand used in the synthesis (Figure 2). The results clearly showed that the quinone moiety was preserved in the framework (a strong C=O stretch band at 1668 cm^{-1}). Additionally, new bands in the 600–400 cm^{-1} region, which can be assigned to the ν(Mn–O) and ν(Mn–N) stretching vibrations, were observed. In the 3750–3000 cm^{-1} region broad, medium intense bands attributed to the ν(OH) vibrations of water and OH ligands were detected. These values are in agreement with data reported in literature for similar Mn(II) complexes.[23]

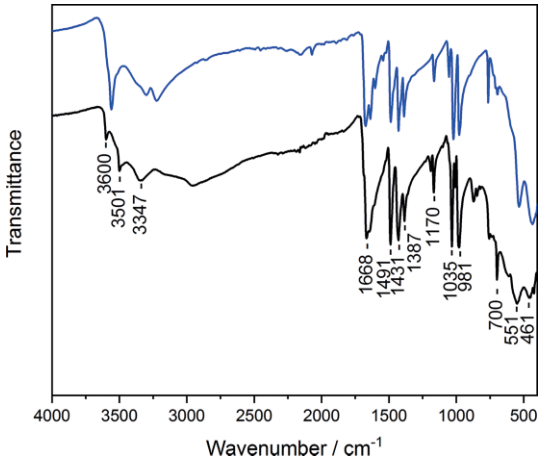

Figure 2. FTIR spectra of the Mn(II) coordination framework (black) and the disodium salt of [1,2,3]triazolo[4,5-*f*]benzotriazole-4,8(2H,6*H*)-dione (ligand **2**, blue).

Single Crystal Structure Analysis

Single crystal X-ray diffraction analysis revealed that the Mn(II) coordination framework $[Mn_3(C_6N_6O_2)_2(OH)_2(H_2O)_4]$ crystallizes in the monoclinic crystal system in the space group $P2_1/n$ (no. 14, Table 1). The asymmetric unit consists of two Mn(II) ions, six nitrogen atoms, six carbon atoms, five oxygen and five hydrogen atoms. An ORTEP-style plot of the asymmetric unit of $[Mn_3(C_6N_6O_2)_2(OH)_2(H_2O)_4]$ is shown in Figure S2 (Supporting information). The atomic coordinates and anisotropic displacement parameters, bond lengths and angles are presented in Tables S1–S4 (Supporting information).

Table 1. Crystallographic parameters and structure refinement details of the Mn(II) coordination framework.

Compound	Mn(II) coordination framework
Empirical formula	$C_{12}H_{10}Mn_3N_{12}O_{10}$
Formula weight	647.10
T /K	100(2)
λ /Å	0.71073
Crystal system	Monoclinic
Space group	$P2_1/n$ (no. 14)
a /Å	6.9177(2)
b /Å	8.8802(2)
c /Å	15.1947(4)
$\alpha = \gamma$ /°	90
β /°	98.1420(10)
Volume /Å^3	924.01(4)
Z	2
Density /g cm^{-3} (calc.)	2.326
Absorption coeff. /mm^{-1}	2.113
F(000)	642
Theta range /°	3.09 to 33.81
Reflections collected	24016
Independent reflections	3710
Refinement method	Full-matrix least-squares on F^2
Data/restraints/parameters	3710/5/189
R(int)	0.0510
GooF	1.040
R_1 [$I > 2\sigma(I)$][a]	0.0297
wR_2 (all data)[b]	0.0651
Largest diff. peak and hole /Å^{-3}	0.618 and −0.532

[a] $R_1 = \Sigma||F_o| - |F_c||/\Sigma|F_o|$. [b] $wR_2 = \Sigma[w(F_o^2 - Fc^2)_2]/\Sigma[w(F_o^2)_2]^{1/2}$.

$[Mn_3(C_6N_6O_2)_2(OH)_2(H_2O)_4]$ features a 2-D layered structure. The layers, parallel to the (001) plane, are created by zig-zag chains of Mn(II) octahedra expanding in *a*-direction and organic ligands. The Mn(II) ions have a distorted octahedral coordination geometry with two different coordination environments. The Mn(1) atom, at sites of $\bar{1}$ symmetry, contains two short equidistant bonds to hydroxido ligands [Mn(1)–O(3), 2.1766(11)] and four long bonds to four different organic ligands via two N(1) and two N(5) donor atoms [Mn(1)–N(1, 5) 2.2918(13)–2.3219(13), Table 2]. Mn(2) atom forms coordinate bonds with two different organic ligands via N(2) and N(4) donor atoms, two aqua ligands and two hydroxido ligands. Within the zig-zag chains, two Mn(2) octahedra are edge sharing and additionally, they are connected by a corner with one Mn(1) octahedron which is further connected with two other Mn(2) octahedra. This Mn(II)-chain is expanding in *a*-direction.

The organic ligand(2–) coordinates in a μ_4-fashion. It forms four coordinate bonds with four Mn(II) ions via N(1), N(2), N(4)

Table 2. Selected bond lengths [Å] found in the Mn(II) coordination framework.

Mn(1)–O(3)	2.1766(11)	Mn(2)–O(4)	2.1318(12)
Mn(1)–O(3)#1	2.1766(11)	Mn(2)–O(5)	2.1728(12)
Mn(1)–N(5)#2	2.2918(13)	Mn(2)–O(3)#5	2.1930(11)
Mn(1)–N(5)#3	2.2918(13)	Mn(2)–O(3)	2.1942(11)
Mn(1)–N(1)#4	2.3219(13)	Mn(2)–N(2)	2.2376(13)
Mn(1)–N(1)#5	2.3219(13)	Mn(2)–N(4)#6	2.3446(13)

Symmetry transformations used to generate equivalent atoms:
#1 –*x* + 2, –*y* + 1, –*z* + 1; #2 –*x* + 1, –*y* + 2, –*z* + 1; #3 *x* + 1, *y* – 1, *z*; #4 *x* + 1, *y*, *z*; #5 –*x* + 1, –*y* + 1, –*z* + 1; #6 *x*, *y* – 1, *z*.

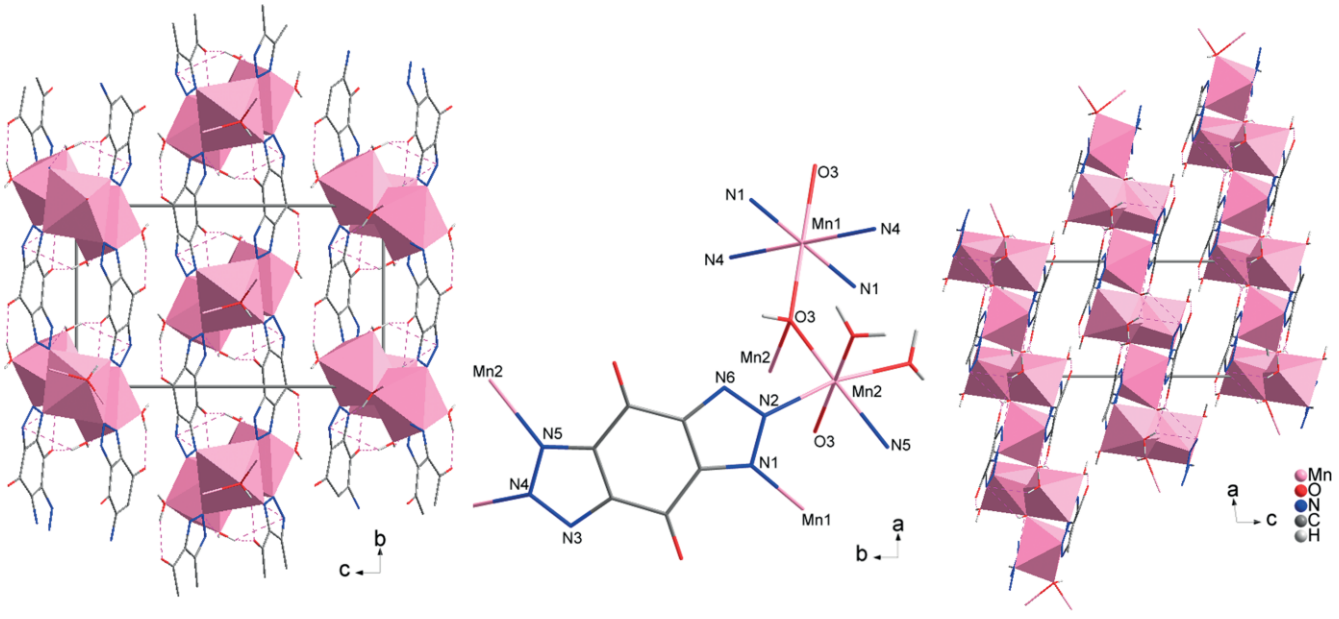

Figure 3. Packing diagram of the Mn(II) coordination framework revealed by single-crystal X-ray analysis viewed in the *a*- (left) and *b*-direction (right) showing selected H-bonds, and a portion of the crystal structure emphasizing the coordination environment of the Mn(1) and Mn(2) ions (middle).

and N(5) donor atoms. The other two ligand N donor atoms [N(3) and N(6)] do not participate in the coordinate bond formation. The molecular packing featuring a 2D-layered structure is shown in Figure 3. The structure of the Mn(II) coordination framework is stabilized by hydrogen bonds between donor hydrogen atoms of aqua and hydroxido ligands, and acceptor oxygen [O(1) and O(2)] and nitrogen [N(6)] atoms of the organic ligand. The list of hydrogen bonds is shown in Table S5 (Supporting information).

The measured X-ray powder diffraction (XRPD) pattern of a bulk sample of the Mn(II) coordination framework shows good agreement with the pattern simulated on the basis of the crystal structure, confirming phase purity of the sample (Figure 4).

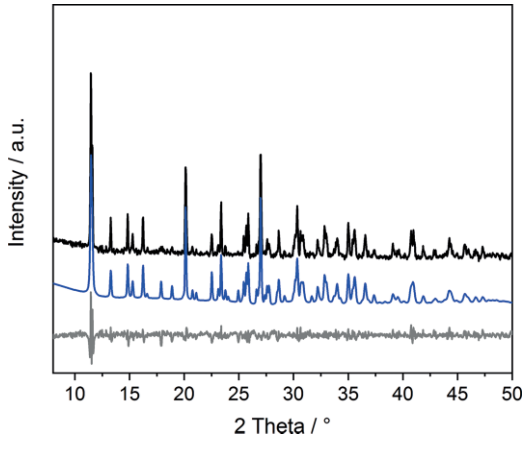

Figure 4. Measured (black) and simulated (Le Bail fit, blue) XRPD patterns of the Mn(II) coordination framework and their difference plot (gray).

Thermal Stability

Thermal stability of the Mn(II) coordination framework was studied by thermogravimetric (TG) analysis and variable temperature XRPD measurement (Figure 5). The XRPD studies reveal that the framework is stable under nitrogen atmosphere up to 250 °C and then decomposes in two steps to form α-Mn_2O_3 (JCPDS no. 41-1442). This result was further confirmed by a TG measurement which also showed a stepwise framework decomposition when heated above 250 °C (Figure 5). To learn more about the framework decomposition, a gas phase formed during the sample heating was analyzed by mass spectrometry (Figure S3, Supporting information). The first mass loss step (from 200 to 400 °C) could be assigned to the removal of four coordinated water molecules and one N_2 molecule from each

ligand (calc.: 19.78 %, found: 19.76 %). The second mass loss (from 400 to 550 °C) is attributed to the further ligand decomposition.

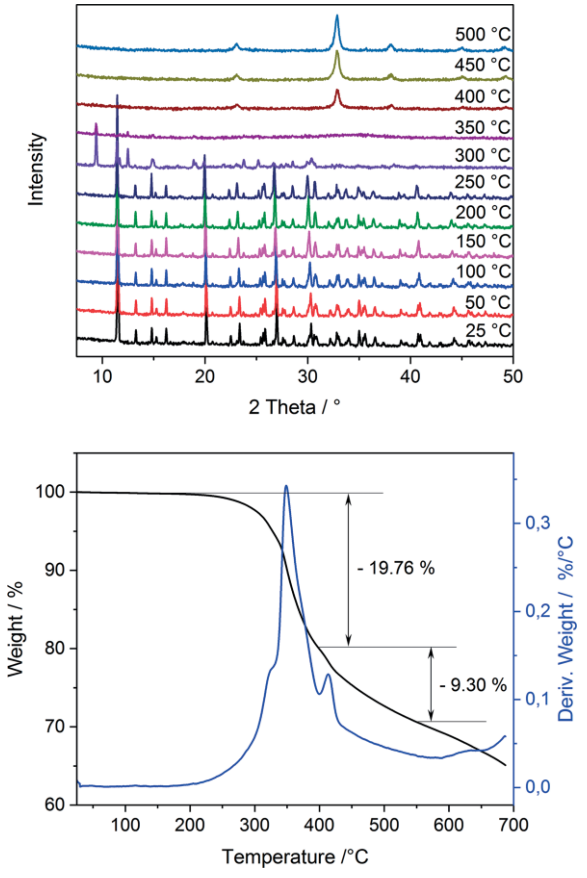

Figure 5. VT XRPD and TG analysis (plotted with a derivative thermogravimetric curve) of the Mn(II) coordination framework meausured under nitrogen atmosphere.

Magnetic Measurements

The magnetic measurements were carried out using a crystalline sample, whose phase purity was confirmed by X-ray powder diffraction analysis (Figure 4). The temperature dependent magnetization of the Mn(II) coordination framework was investigated in the range of 1.8–400 K with applied magnetic fields of 1 and 10 kOe (Figure 6). At elevated temperature $T > 50$ K the inverse susceptibility, shown in the main figure reveals an antiferromagnetic Curie–Weiss law, but turns into ferromagnetic characteristics at low temperatures $T < 50$ K. This is underlined by the χT plot in the lower inset, which starting from high temperature gradually decreases as typical for an antiferromagnet, then abruptly increases below 35 K like in a ferromagnet and finally develops a peak at about 10 K indicating the magnetic ordering transition. Fitting the susceptibility data, by the expression $1/\chi = (T - \Theta)/C - \zeta/(T - \Theta')$ derived from Néel's ferrimagnetic mean-field model,[24] yields an antiferromagnetic Curie–Weiss temperature of $\Theta = -71.6(6)$ K and a Curie constant $C = 12.8(2)$ (emu K)/mol, while the ferromagnetic deviation is parametrized by $\zeta = 19(1)$ (mol K)/emu and $\Theta' = 18.5(4)$ K. From $C = N_A \cdot \mu_B^2 \cdot p_{eff}^2/(3k_B)$, where N_A, μ_B, and k_B denote the Avogadro number, Bohr magneton and Boltzmann constant, respectively, one derives an effective moment $p_{eff} = 10.12$, which is in nice agreement with the value $[3 \cdot g^2 \cdot S \cdot (S + 1)]^{1/2} = 10.25$ expected for three Mn^{2+} spins $S = 5/2$ (electronic configuration $3d^5$, g-value $g = 2$) per formula unit. At low temperatures the magnetization (cf. upper inset) saturates at about 5 μ_B per formula unit proving the ferrimagnetic alignment of two manganese sublattices with ratio 2:1. This is further corroborated by the field-dependent magnetization loops recorded at different temperatures as shown in the main frame of Figure 7. At 2 K we observe a narrow hysteresis loop typical for a soft magnet saturating already at 10 kOe at a value slightly below 5 μ_B per for-

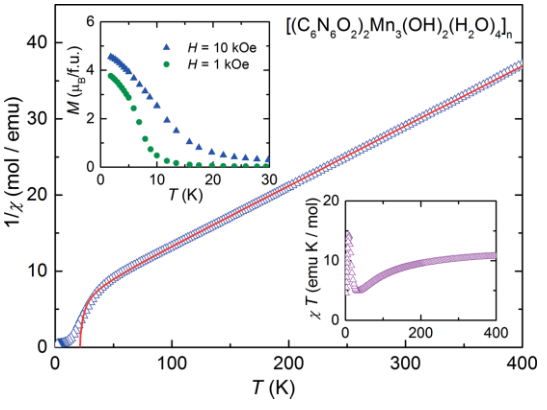

Figure 6. Main figure. Temperature dependent susceptibility $\chi(T) = M/H$ of the Mn(II) coordination framework in inverse representation, as measured in a magnetic field $H = 10$ kOe. The red solid line indicates a fit by a ferrimagnetic mean-field model as described in the text. Upper inset: temperature dependence of the magnetization M around the ferrimagnetic transition at magnetic fields of 1 kOe (green circles) and 10 kOe (blue triangles). Lower inset: temperature dependence of the product χ^*T.

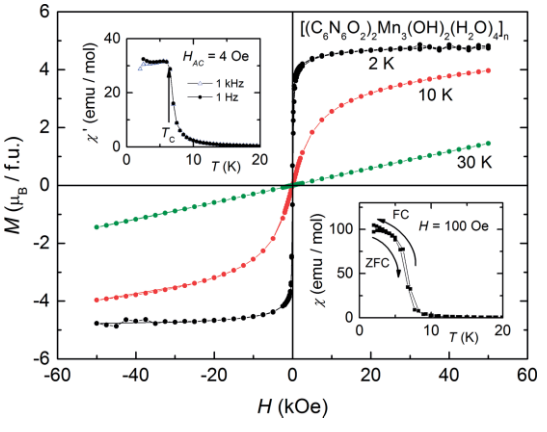

Figure 7. Main frame: magnetization M of the Mn(II) coordination framework as function of the external magnetic field H for selected temperatures above (30 K, 10 K) and below (2 K) the ferrimagnetic transition at $T_C = 6.5$ K. At 2 K saturation is approached already above 10 kOe. Upper inset: temperature dependence of the AC susceptibility measured with an AC field amplitude of $H_{AC} = 4$ Oe at frequencies of 1 Hz and 1 kHz. The Curie temperature T_C is obtained from the kink at $T_C = 6.5$ K. Lower inset: temperature dependent field-cooled (FC) and zero-field cooled (ZFC) susceptibilities measured in an external static field of $H = 100$ Oe. Weak splitting due to domain effects shows up below 4 K.

mula unit. To localize the magnetic phase transition more accurately, the upper inset in Figure 7 shows AC susceptibility data, which indicate the Curie temperature by the kink at about T_C = 6.5 K. This is also in line with the field-cooled-(FC) vs. zero-field cooled (ZFC) susceptibilities taken at a small external field of 100 Oe as shown in the lower inset of Figure 7.

Conclusions

As reported in literature, by combining Mn(II) cations and bistriazole ligands, MOFs with honeycomb-like structure were prepared.[12,13] Inspired by these results, we combined a redox-active bistriazole ligand, [1,2,3]triazolo[4,5-*f*]benzotriazole-4,8(2H,6*H*)-dione, with Mn(II) cations to prepare a potentially redox-active MOFs. To our surprise instead of a MOF, we obtained a 2D-layered structure formed by the bistriazolate ligands coordinating in a μ_4-fashion to Mn(II)-cations (instead of the expected μ_6-fashion). The thermal stability studies revealed that the framework is stable up to 250 °C. Magnetic measurements show that in the paramagnetic regime the magnetization of the Mn(II) coordination framework is well described in terms of a ferrimagnetic mean-field model. Long-range ferrimagnetic order sets in at about 6.5 K.

If we use Co(II) or Ni(II) salts instead of Mn(II) salts and carry out the same synthesis procedure, we are able to prepare Co(II) and Ni(II)-MOFs with the expected honeycomb-like structure and the prepared materials are currently the subject of our investigation. However, despite all our efforts, until now the analogues MOF containing Mn(II) cations could not be obtained. With regard to the unexpected structural features, material thermal stability and magnetic properties of the Mn(II) coordination framework, this work shows that coordination polymers based on functionalized triazolate ligands could be promising candidates for preparing materials with intriguing structural and magnetic properties. Work along this line is currently in progress in our lab.

Experimental Section

Materials and Methods: All reagents were of analytical grade and used as received from commercial suppliers except [1,2,3]triazolo[4,5-*f*]benzotriazole-4,8(2H,6*H*)-dione which was prepared by procedures reported previously.[11] Optical microscopy images were taken using an Olympus IX70 microscope equipped with a camera. Fourier transform infrared (FT-IR) spectra were recorded with an ATR unit in the range 4000–400 cm^{-1} on a Bruker Equinox 55 FT-IR spectrometer. Thermogravimetric (TG) analysis was performed with a TG Q500 analyzer in the temperature range of 25–700 °C under a nitrogen atmosphere at a heating rate of 5 K min^{-1}. To analyze the gas phase, a BelCat-B catalyst analyzer (Bel Japan, Inc.) coupled with a mass spectrometer (OmniStar GSD 320, Pfeiffer Vacuum) was used. The sample was placed between two plugs of quartz wool in a quartz glass reactor and heated up to 550 °C (5 K min^{-1}) under a flow of argon (30 mL min^{-1}). The composition of the exhaust gas was analyzed by a mass spectrometer. X-ray powder diffraction data were collected in the 5–50° 2θ range using a Seifert XRD 3003 TT – powder diffractometer with a Meteor1D detector operating at room temperature using Cu-$K_{\alpha1}$ radiation (λ = 1.54187). VT XRPD data were collected on a Panalytical Empyrean diffractometer in transmittance Bragg–Brentano geometry employing Cu-radiation. The patterns were recorded in a temperature range of 25 to 500 °C, in the 5–50° 2θ range with a step time of 1 s and a step width of 0.02° 2θ. Temperature program between measurements: 0.5 °C s^{-1} heating rate, followed by 10 min isothermal steps required for recording diffraction data sets. The sample was exposed to a nitrogen atmosphere during the measurements. Magnetic properties were investigated with a Quantum Design MPMS 5 SQUID magnetometer applying field cooling with liquid helium. Susceptibility measurements were performed in a temperature range from 1.8 to 400 K and in external fields *H* of 0.1, 1 and 10 kOe, as well as AC susceptibility in an AC field of 4 Oe amplitude and at AC frequencies between 1 Hz and 1 kHz. Magnetization loops were recorded at constant temperature in a field range between –50 kOe and +50 kOe. For the single-crystal X-ray analysis, a crystal of the Mn(II) coordination framework was taken from mother liquor and mounted on a MiTeGen MicroMounts. The data for the structure determination were collected on a Bruker D8 Venture diffractometer. Intensity measurements were performed using monochromated (doubly curved silicon crystal) Mo-K_α radiation (0.71073 Å) from a sealed microfocus tube. Generator settings were 50 kV, 1 mA. APEX3 software was used for preliminary determination of the unit cell.[25] Determination of integrated intensities and a unit cell refinement were performed using SAINT.[26] The structure was solved using the Bruker SHELXTL Software Package and refined using SHELXL.[27,28] Selected crystal data and details of the structure refinement are provided in Table 1. Non-hydrogen atoms were refined with anisotropic temperature parameters.

CCDC 1942394 {for the Mn(II) coordination framework} contains the supplementary crystallographic data for this paper. These data can be obtained free of charge from The Cambridge Crystallographic Data Centre.

Synthesis of the Mn Coordination Framework: The disodium salt of [1,2,3]triazolo[4,5-*f*]benzotriazole-4,8(2H,6*H*)-dione [$Na_2(C_6N_6O_2)$·$4H_2O$, 40 mg, 0.131 mmol], prepared according a previously reported procedure,[11] and $MnCl_2$·$4H_2O$ (60 mg, 0.303 mmol) were dissolved in water (4 mL). The mixture was sealed in a glass heating tube and heated at 100 °C for 16 h. Upon slow cooling down, the formed light yellow-orange crystals were collected via filtration, washed well with hot water and dried on air to give 26.7 mg of the product [63.2 %, calcd. for $(C_6N_6O_2)_2Mn_3(OH)_2(H_2O)_4$]. The same material was obtained when $MnBr_2$·$4H_2O$ (0.303 mmol) or $Mn(OAc)_2$·$4H_2O$ (0.303 mmol) were used as metal salts instead of $MnCl_2$·$4H_2O$. FTIR: $\tilde{\nu}$ = 3600, 3501, 3347, 2953, 1668, 1491, 1431, 1387, 1191, 1170, 1035, 1010, 981, 873, 848, 758, 700, 551, 461, 425 cm^{-1}.

Acknowledgments

The authors are grateful to A. Kalytta-Mewes and Dr. M. Kraft from the Institute of Physics, University of Augsburg, for their help with carrying out the XRPD analysis, and to D. Vieweg (EP V, University of Augsburg) for the SQUID measurement. H.-A. K. v. N. acknowledges financial support by the German Research Foundation (DFG) – grant no. 107745057 – TRR 80 "From Electronic Correlations to Functionality" (Augsburg, Munich, Stuttgart).

Keywords: Manganese · N ligands · Quinones · Coordination polymers · 1,2,3-Triazole

[1] B. Schulze, U. S. Schubert, *Chem. Soc. Rev.* **2014**, *43*, 2522–2571.
[2] G. Aromí, L. A. Barrios, O. Roubeau, P. Gamez, *Coord. Chem. Rev.* **2011**, *255*, 485–546.
[3] D. A. Reed, B. K. Keitz, J. Oktawiec, J. A. Mason, T. Runčevski, D. J. Xiao, L. E. Darago, V. Crocellà, S. Bordiga, J. R. Long, *Nature* **2017**, *550*, 96–100.
[4] P. Schmieder, M. Grzywa, D. Denysenko, M. Hambach, D. Volkmer, *Dalton Trans.* **2015**, *44*, 13060–13070.
[5] P. Schmieder, D. Denysenko, M. Grzywa, B. Baumgärtner, I. Senkovska, S. Kaskel, G. Sastre, L. van Wüllen, D. Volkmer, *Dalton Trans.* **2013**, *42*, 10786–10797.
[6] C.-Z. Ruan, R. Wen, M.-X. Liang, X.-J. Kong, Y.-P. Ren, L.-S. Long, R.-B. Huang, L.-S. Zheng, *Inorg. Chem.* **2012**, *51*, 7587–7591.
[7] F. Gandara, F. J. Uribe-Romo, D. K. Britt, H. Furukawa, L. Lei, R. Cheng, X. Duan, M. O'Keeffe, O. M. Yaghi, *Chem. Eur. J.* **2012**, *18*, 10595–10601.
[8] D. Denysenko, M. Grzywa, M. Tonigold, B. Streppel, I. Krkljus, M. Hirscher, E. Mugnaioli, U. Kolb, J. Hanss, D. Volkmer, *Chem. Eur. J.* **2011**, *17*, 1837–1848.
[9] A. Demessence, D. M. D'Alessandro, M. L. Foo, J. R. Long, *J. Am. Chem. Soc.* **2009**, *131*, 8784–8786.
[10] S. Biswas, M. Grzywa, H. P. Nayek, S. Dehnen, I. Senkovska, S. Kaskel, D. Volkmer, *Dalton Trans.* **2009**, 6487–6495.
[11] H. Bunzen, A. Lamp, M. Grzywa, C. Barkschat, D. Volkmer, *Dalton Trans.* **2017**, *46*, 12537–12543.
[12] P.-Q. Liao, X.-Y. Li, J. Bai, C.-T. He, D.-D. Zhou, W.-X. Zhang, J.-P. Zhang, X.-M. Chen, *Chem. Eur. J.* **2014**, *20*, 11303–11307.
[13] A. J. Rieth, Y. Tulchinsky, M. Dincă, *J. Am. Chem. Soc.* **2016**, *138*, 9401–9404.
[14] J.-J. Liu, C.-X. He, F.-X. Cheng, C.-C. Huang, *Z. Anorg. Allg. Chem.* **2017**, *643*, 548–552.
[15] Z.-B. Han, R.-Y. Lu, Y.-F. Liang, Y.-L. Zhou, Q. Chen, M.-H. Zeng, *Inorg. Chem.* **2012**, *51*, 674–679.
[16] D.-F. Weng, Z.-M. Wang, S. Gao, *Chem. Soc. Rev.* **2011**, *40*, 3157–3181.
[17] Y. Journaux, J. Ferrando-Soria, E. Pardo, R. Ruiz-Garcia, M. Julve, F. Lloret, J. Cano, Y. Li, L. Lisnard, P. Yu, H. Stumpf, C. L. M. Pereira, *Eur. J. Inorg. Chem.* **2018**, *2018*, 228–247.
[18] Q. Yue, E.-Q. Gao, *Coord. Chem. Rev.* **2019**, *382*, 1–31.
[19] D. Maspoch, D. Ruiz-Molina, J. Veciana, *Chem. Soc. Rev.* **2007**, *36*, 770–818.
[20] G. M. Espallargas, E. Coronado, *Chem. Soc. Rev.* **2018**, *47*, 533–557.
[21] K. S. Park, Z. Ni, A. P. Côté, J. Y. Choi, R. Huang, F. J. Uribe-Romo, H. K. Chae, M. O'Keeffe, O. M. Yaghi, *Proc. Natl. Acad. Sci. USA* **2006**, *103*, 10186–10191.
[22] A. Phan, C. J. Doonan, F. J. Uribe-Romo, C. B. Knobler, M. O'Keeffe, O. M. Yaghi, *Acc. Chem. Res.* **2010**, *43*, 58–67.
[23] N. Turan, R. Adigüzel, K. Buldurun, E. Bursal, *Int. J. Pharmacol.* **2016**, *12*, 92–100.
[24] J. S. Smart, *Am. J. Phys.* **1955**, *23*, 356–370.
[25] *APEX3* Version **2016**.9, Bruker AXS Inc.
[26] *SAINT* Version 8.37A, **2015**, Bruker AXS Inc.
[27] G. M. Sheldrick, *Acta Crystallogr., Sect. A* **2008**, *64*, 112–122.
[28] G. M. Sheldrick, *Acta Crystallogr., Sect. C* **2015**, *71*, 3–8.

Received: July 23, 2019